Organic & Biomolecular Chemistry

www.rsc.org/obc

Volume 7 | Number 8 | 21 April 2009 | Pages 1485–1736

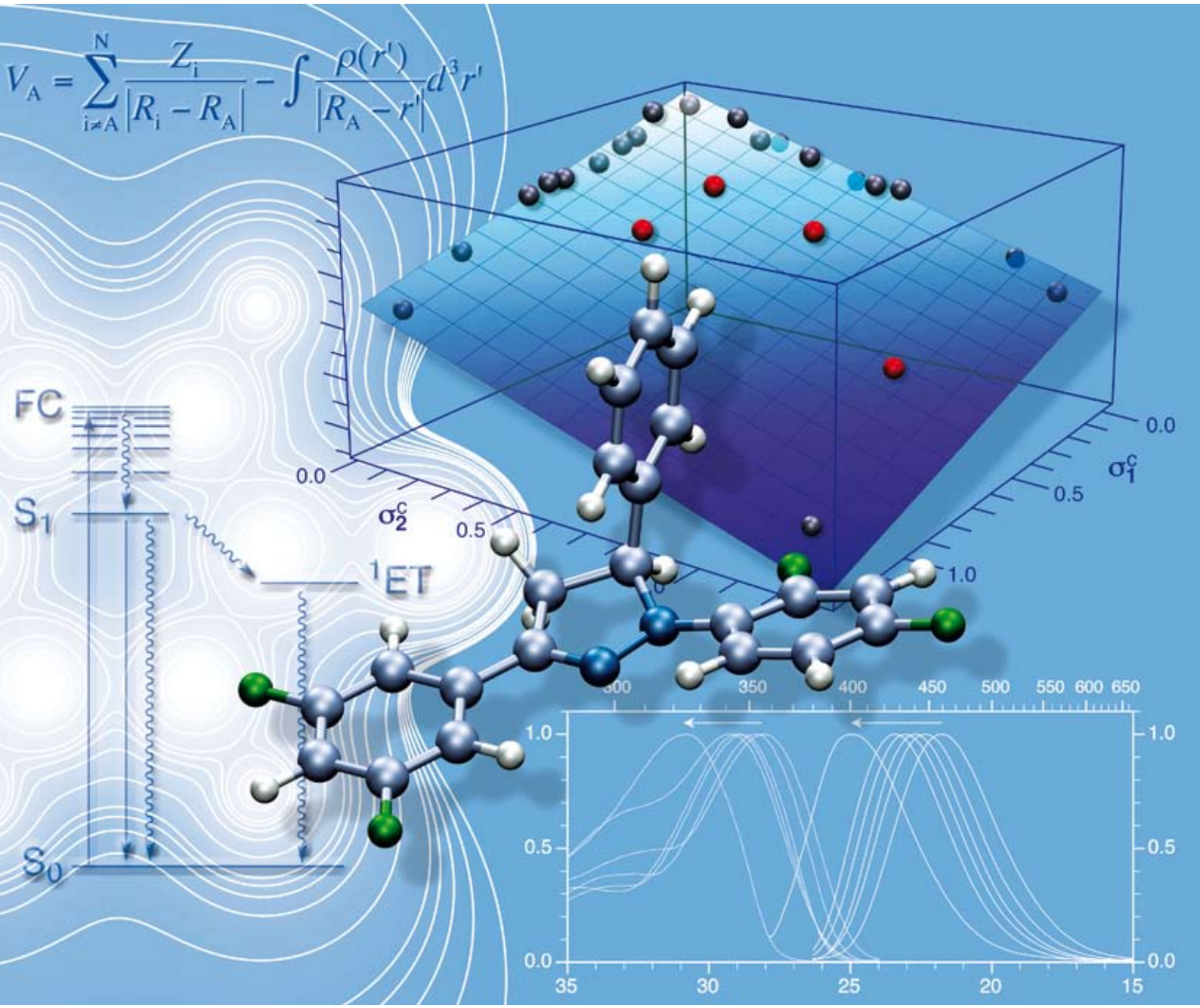

ISSN 1477-0520

RSC Publishing

FULL PAPER

Manjusha Verma *et al.*

Predicting photoinduced electron transfer thermodynamics in polyfluorinated 1,3,5-triarylpyrazolines based on multiple linear free energy relationships

Chemical Science

In this issue...

1477-0520(2009)7:8;1-7

Predicting the photoinduced electron transfer thermodynamics in polyfluorinated 1,3,5-triarylpyrazolines based on multiple linear free energy relationships†

Manjusha Verma, Aneese F. Chaudhry and Christoph J. Fahrni*

Received 25th November 2008, Accepted 9th January 2009
First published as an Advance Article on the web 20th February 2009
DOI: 10.1039/b821042j

The photophysical properties of 1,3,5-triarylpyrazolines are strongly influenced by the nature and position of substituents attached to the aryl-rings, rendering this fluorophore platform well suited for the design of fluorescent probes utilizing a photoinduced electron transfer (PET) switching mechanism. To explore the tunability of two key parameters that govern the PET thermodynamics, the excited state energy ΔE_{00} and the acceptor potential $E(A/A^-)$, a library of polyfluoro-substituted 1,3-diaryl-5-phenyl-pyrazolines was synthesized and characterized. The observed trends for the PET parameters were effectively captured through multiple Hammett linear free energy relationships (LFER) using a set of independent substituent constants for each of the two aryl rings. Given the lack of experimental Hammett constants for polyfluoro-substituted aromatics, theoretically derived constants based on the electrostatic potential at the nucleus (EPN) of carbon atoms were employed as quantum chemical descriptors. The performance of the LFER was evaluated with a set of compounds that were not included in the training set, yielding a mean unsigned error of 0.05 eV for the prediction of the combined PET parameters. The outlined LFER approach should be well suited for designing and optimizing the performance of cation-responsive 1,3,5-triarylpyrazolines.

Introduction

Photoinduced electron transfer (PET) is a fundamental photophysical process that plays a key role in a broad range of synthetic and natural systems.[1] In the initial step of PET, a photon is absorbed by a fluorophore yielding a photoexcited state with dramatically altered redox properties. If a suitable electron donor or acceptor is present, an electron transfer step follows in which the photoexcited state is acting either as a reductant or an oxidant. In the final step, the formed radical ion pair undergoes charge recombination to return to the initial ground state. Because charge recombination is typically a non-radiative process, PET acts as a fluorescence quenching pathway.[1] This property has been extensively utilized for the design of fluorescent probes, which upon binding to an analyte yield a change in emission intensity.[2,3] The fluorescence response of the probe is governed by the relative rates of electron transfer in the presence and absence of the analyte. If the quenching electron donor is only weakly coupled to the excited fluorophore, the electron transfer occurs in the nonadiabatic regime and is best described by the semiclassical Marcus theory.[4,5] Within this framework, the ET kinetics depends on the thermodynamic driving force of the ET reaction, the associated reorganization energy, and the electronic coupling between the excited fluorophore and the successor radical ion pair. The driving force of the ET reaction ($-\Delta G_{et}$) can be estimated based on the Rehm-Weller eqn (1),

$$\Delta G_{et} = E(D^+/D) - E(A/A^-) - \Delta E_{00} + w_p \quad (1)$$

where $E(D^+/D)$ and $E(A/A^-)$ correspond to the donor and acceptor ground state potentials, respectively, ΔE_{00} is the transition energy between the vibrationally relaxed ground and excited states of the fluorophore, and w_p is the Coulomb stabilization energy associated with the intermediate radical ion pair.[6] The Rehm-Weller formalism therefore offers a rational basis for tuning the PET driving force and thus the kinetics of the ET reaction.

Tuning the PET thermodynamics is vital for optimizing the contrast ratio of metal cation responsive PET sensors.[7–9] In this application of PET, the cation receptor is typically acting as the electron donor and the excited fluorophore as the electron acceptor. Since the donor potential $E(D^+/D)$ is determined by the choice of the receptor moiety, the remaining parameters for adjusting the ET driving force according to eqn (1) are the excited state energy ΔE_{00} of the fluorophore and its reduction potential $E(A/A^-)$. Because both of these parameters intrinsically depend on the fluorophore structure, it is generally not possible to selectively tune one without altering the other. Owing to their unusual electronic structure, 1,3,5-triarylpyrazoline fluorophores represent a welcome exception.[10–12] This fluorophore platform is composed of two aryl-rings that are connected through a central pyrazoline core (Chart 1). Due to significant spatial separation of the HOMO and LUMO densities, substituents attached to the 1-aryl ring primarily influence the fluorophore excited state energy without significantly affecting its reduction potential.[11] The third aryl ring in the 5-position is connected through an sp^3-hybridized carbon and is electronically decoupled from the fluorophore π-system, thus offering a convenient handle for attaching a metal ion receptor.

School of Chemistry and Biochemistry, Petit Institute for Bioengineering and Bioscience, Georgia Institute of Technology, 901 Atlantic Drive, Atlanta, Georgia 30332, U.S.A.. E-mail: fahrni@chemistry.gatech.edu

† Electronic supplementary information (ESI) available: Computational data. See DOI: 10.1039/b821042j

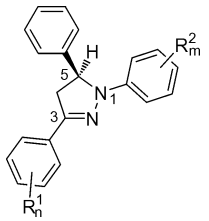

Chart 1

To optimize the contrast ratio of the probe response in a systematic and rational way, we have recently utilized linear free energy relationships (LFERs) to correlate quantum chemical parameters of 1,3,5-triarylpyrazoline fluorophores with their experimental PET thermodynamics.[10] The correlation yielded an average unsigned error of less than 0.03 eV over 20 structurally distinct fluorophores. While inherently limited to the experimental conditions utilized to generate the LFER, the approach is principally suitable to predict the PET thermodynamics for a broad range of pyrazoline fluorophores.

Quantitative structure–property and structure–activity correlations are powerful tools for designing molecules with tailored properties. In particular, Hammett substituent constants (σ)[13] have been widely used by organic chemists to quantify the electron withdrawing and donating abilities of substituents in relation to chemical reactivity or molecular properties such as aromaticity, pK_a, proton NMR shifts, or infrared vibrational energies.[14–18] Given the observation that in 1,3,5-triarylpyrazolines the excited state energy and the acceptor potential, two of the key parameters for adjusting the PET thermodynamics, are strongly influenced by the nature of the substituents R^1 and R^2,[10,11] we envisioned that a set of two Hammett constants might already be sufficient to capture the substituent effects and thus to predict the photophysical properties of a particular derivative. In this way, the two Hammett constants represent two independent variables of a regression plane that correlate the substituent effects with these two thermodyamic parameters.

To alter the electron withdrawing or donating ability of the 1- and 3-aryl rings, any combination of substituents R^1 and R^2 would be suitable; however, we aimed at minimizing potential irregularities in the LFER, for example those caused by strong resonance contributions, and therefore, we restricted the choice of substituents to a single type. The electronic properties can then be readily tuned by changing the number and position of substituents on each aryl ring. Recent studies have demonstrated that the electronic effects of fluoro substituents are additive,[19,20] thus rendering them well suited for this purpose.

To derive Hammett constants of polyfluorinated rings, the contribution of each substituent could be principally captured by summing up the individual constants. While Hammett constants are reliably established for meta and para substituted aromatics, capturing the effects of ortho substituents remains a challenging problem.[21–23] Because steric interactions and proximity effects are specific to the nature of the neighboring ortho substituents, experimental data obtained for one class of molecules cannot be directly applied to another class. For this reason, we decided to derive the Hammett constants for polyfluoro-substituted benzenes on the basis of quantum chemical calculations. This approach has the advantage that the overall electronic contribution of the substituent ensemble is captured in an unbiased manner, and that potential steric effects specific to the pyrazoline fluorophore architecture can be later evaluated on the basis of the LFER. A number of studies showed that several quantum chemical parameters linearly correlate with experimentally derived Hammett constants.[18,24–29] Recently, Galabov *et al.* demonstrated that the theoretical electrostatic potentials at the nuclei (EPN) of carbon atoms in substituted benzenes represent an excellent reactivity descriptor.[30] The electrostatic potential V_A at a particular nucleus (A) in a molecule with N nuclei can be readily obtained from the molecular electrostatic potential by leaving out the contribution due to the charge Z_A on nucleus A, thus yielding eqn (2),

$$V_A = \sum_{i \neq A}^{N} \frac{Z_i}{|R_i - R_A|} - \int \frac{\rho(r')}{|R_A - r'|} d^3r' \quad (2)$$

where Z_i and R_i are the charge and radius vectors of the nucleus i, respectively, ρ is the electron-density of the molecule, and r' is a dummy integration variable.[31] The theoretically estimated EPN values based on eqn (2) and the experimental Hammett constants σ^0 for 29 substituted benzenes yielded a linear regression eqn (3a) with an excellent correlation coefficient of $r = 0.993$ (with V_C corresponding to the carbon EPN values in atomic units).[30]

$$V_C = 0.044\ \sigma^0 - 14.777 \quad (3a)$$

$$\sigma^c = (V_C + 14.777)/0.044 \quad (3b)$$

Given the linear relationship (3a), computational potentials V_C should principally be suitable to predict Hammett constants of substituted benzenes for which no experimental data are available (eqn 3b). Encouraged by this report, we decided to explore whether an LFER based on computational substituent constants σ^c might be sufficient to predict the PET thermodynamics in 1,3,5-triarylpyrazolines. To this end, we first calculated the EPN values for a series of polyfluoro-substituted benzenes, derived the corresponding theoretical Hammett constants σ^c according to eqn (3b), and then utilized the experimental photophysical data of 20 polyfluoro-substituted triarylpyrazolines as a training set to establish Hammett LFERs for the excited state energy ΔE_{00} and the acceptor potential $E(A/A^-)$, two of the key PET parameters (eqn 1). Finally, we evaluated the performance of the LFERs by predicting the photophysical properties for a set of compounds that were not included in the initial training set.

Results and discussion

Theoretical Hammett constants for polysubstituted benzenes

There are a total of 19 possible ways to attach between 1 and 5 fluoro substituents to a single aryl ring. With the inclusion of the unsubstituted aryl ring, it would therefore be possible to construct 400 different 1,3-diaryl substituted pyrazolines. Although each of the 19 fluoroaryl rings should exhibit distinct electronic properties, it is still possible that some of these derivatives are quite similar. To construct a balanced LFER training set, a broad and equally spaced distribution of Hammett constants would be desirable. Therefore, we first calculated the theoretical EPN for all possible fluorobenzenes, and predicted the corresponding Hammett constants σ^c based on eqn (3b). Each derivative was

Table 1 Theoretical Hammett substituent constants σ^c for mono- and polysubstituted fluorobenzenes

Substituent	V_c/au[a]	$\sigma^{c\,b}$	$\Sigma\sigma^{c\,c}$	pK_a[d]
H	−14.77568	0.03	0.03	9.99[e]
2-F	−14.76462	0.28	0.28	8.73[e]
3-F	−14.76191	0.34	0.34	9.28[e]
4-F	−14.76832	0.20	0.20	9.95[f]
2,3-F_2	−14.75277	0.55	0.62	–
3,4-F_2	−14.75561	0.49	0.54	–
2,4-F_2	−14.75760	0.44	0.48	8.58[e]
2,6-F_2	−14.75357	0.53	0.56	7.51[e]
3,5-F_2	−14.74826	0.65	0.68	8.4[g]
2,5-F_2	−14.75083	0.59	0.62	7.7[g]
2,3,4-F_3	−14.74654	0.69	0.82	–
3,4,5-F_3	−14.74266	0.78	0.88	–
2,3,5-F_3	−14.73933	0.86	0.96	–
2,4,5-F_3	−14.74482	0.73	0.82	7.7[g]
2,3,6-F_3	−14.74145	0.81	0.90	–
2,4,6-F_3	−14.74704	0.68	0.76	–
2,3,4,5-F_4	−14.73391	0.98	1.16	–
2,3,4,6-F_4	−14.73598	0.93	1.10	–
2,3,5,6-F_4	−14.72994	1.07	1.24	6.00[e]
2,3,4,5,6-F_5	−14.72481	1.19	1.44	5.53[e]

[a] Electrostatic potential V at nucleus C1 in atomic units (numbering scheme according to Fig. 1). [b] Theoretical substituent constants based on eqn (3b). [c] Additive substituent constant based on the sum of the corresponding theoretical ortho (0.28), meta (0.34), and para (0.20) constants. [d] Published acidity constants of the corresponding fluoro-substituted phenols: [e] from reference 32, [f] from reference 33, [g] from reference 34.

geometry optimized using density functional theory with the B3LYP hybrid functional and the 6-311+G(2d,2p) basis set. The presence of a true stationary point on the respective potential energy surface was confirmed based on harmonic vibrational frequency calculations. An overview of the computational results, including the EPN values V_C at carbon C1 and the corresponding predicted Hammett constants are compiled in Table 1.

To distinguish from experimentally derived constants, all computational Hammett constants are referenced as σ^c throughout this text. As apparent from Table 1, the σ^c values are gradually increasing with an increasing number of fluoro substituents, thus directly reflecting the change in electron withdrawing ability of the aryl ring. The pentafluoro-substituted ring has a σ^c constant of 1.19, which is greater than the experimental constant of very strongly electron withdrawing substituents such as –C(CN)=C(CN)$_2$ (0.98) or –SO$_2$C(CF$_3$)$_3$ (1.13).[13] To evaluate the additivity of the electron withdrawing contributions of each substituent, we also derived Hammett constants as the sum of the corresponding theoretical ortho, meta, and para substituent constants. For example, the expected constant of the pentafluoro-substituted ring according to this scheme was obtained as the sum of 2 ortho (0.28), 2 meta (0.34), and 1 para (0.20) contributions. As evident from Table 1, the additive constants are consistently larger compared to the σ^c values, indicating the presence of some proximity effects. Nevertheless, linear regression analysis of the two data sets yielded an excellent correlation coefficient of r = 0.996 and a slope of 0.79 (Fig. 1). The latter indicates that compared to the corresponding mono-substituted derivatives, the electron withdrawing ability is reduced by approximately 20% with each additional fluoro substituent; however, given the linearity of the correlation, there is no apparent saturation effect, even in the case of the crowded pentafluoro aryl ring.

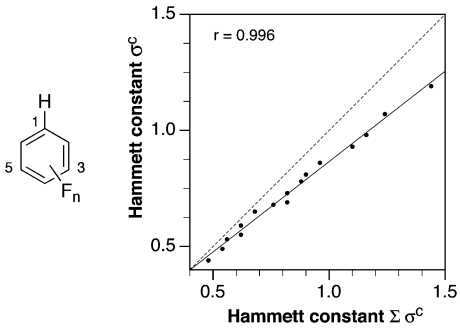

Fig. 1 Linear correlation of the theoretical Hammett constants σ^c calculated according to eqn (3b) of 16 polyfluoro-substituted benzenes (left) and the additive Hammett constants obtained as the sum of the corresponding ortho, meta, and para constants. The dashed line indicates an ideal correlation with a slope of 1.

To evaluate the computational Hammett constants with an actual experimental data set, we then constructed an LFER for all available literature pK_a's of fluoro-substituted phenols (Table 1). The linear regression analysis yielded a correlation coefficient of r = 0.972 over all pK_a's. Most importantly, the correlation remains linear throughout the strongly electron withdrawing pentafluorophenol and does not point towards any saturation effects. Restricting the regression to derivatives that contain at least one ortho fluoro substituent, the correlation slightly improved with r = 0.990. It is not clear to what extent proximity effects are responsible for this observation; resonance effects with the para fluoro substituent might be similarly important. In either case, the computational Hammett constant would not be expected to reflect such contributions, which might become particularly important for the delocalized phenolate anion.

In summary, the derived computational Hammett constants capture the electron withdrawing ability of polyfluoro-substituted aryl rings in a systematic manner. While there remains some uncertainty towards the validity of the absolute values compared to other non-fluoro substituted derivatives, the series appears internally consistent and should therefore be suitable as the basis of a more extended LFER for correlating the photophysical properties of pyrazolines.

Synthesis and characterization of a polyfluoro-substituted 1,3,5-triarylpyrazoline library as an LFER training set

Based on the computational results above, we selected a total of 10 fluoro-substituted aryl rings to design an LFER training set (bold type in Table 1). While in principle any combination of fluoro-substituted aryl rings could be used in the training set, we preferred to include only those containing either substituents on the 1-aryl ring (compounds **1b–1j**) or the 3-aryl ring (compounds **2a–10a**). This approach has the advantages that the influence of each aryl ring can be better traced, and that the quality of the linear correlations can be more readily gauged along a single Hammett constant coordinate. To better define the slope and position of the regression plane, we also included in the training set a derivative with fully perfluorinated aryl rings (compound **10j**). Table 2 provides an overview of all synthesized compounds as well as the associated computational Hammett constants for each aryl ring. To minimize interferences from undesired PET

Table 2 Substituent key and computed Hammett constants σ^c utilized in the LFER study[a]

Entry	Compd	R^1	R^2	$\sigma_1{}^{c\ b}$	$\sigma_2{}^{c\ b}$
1	**1a**	H	H	0.03	0.03
2	**1b**	H	2-F	0.03	0.28
3	**1c**	H	3-F	0.03	0.34
4	**1d**	H	4-F	0.03	0.20
5	**1e**	H	2,4-F_2	0.03	0.44
6	**1f**	H	2,5-F_2	0.03	0.59
7	**1g**	H	3,5-F_2	0.03	0.65
8	**1h**	H	2,4,5-F_3	0.03	0.73
9	**1i**	H	2,3,5,6-F_4	0.03	1.07
10	**1j**	H	2,3,4,5,6-F_5	0.03	1.19
11	**2a**	2-F	H	0.28	0.03
12	**3a**	3-F	H	0.34	0.03
13	**4a**	4-F	H	0.20	0.03
14	**5a**	2,4-F_2	H	0.44	0.03
15	**6a**	2,5-F_2	H	0.59	0.03
16	**7a**	3,5-F_2	H	0.65	0.03
17	**8a**	2,4,5-F_3	H	0.73	0.03
18	**9a**	2,3,5,6-F_4	H	0.98	0.03
19	**10a**	2,3,4,5,6-F_5	H	1.19	0.03
20	**10j**	2,3,4,5,6-F_5	2,3,4,5,6-F_5	1.19	1.19

[a] Computational Hammett constant according to eqn (3b). [b] $\sigma_1{}^c$ and $\sigma_2{}^c$ refer to the respective aryl rings attached to the 3- and 1-position of the central pyrazoline ring.

Table 3 Photophysical data of pyrazoline derivatives **1a–1j**[a], **2a–10a**, and **10j** in acetonitrile (298K)

Compd	abs λ_{max}/nm	em λ_{max}/nm	Stokes shift/cm^{-1}	$\Delta E_{00}{}^b$/ cm^{-1}/eV		$\Phi_F{}^c$
1a	356	459	6300	24 940	3.09	0.65
1b	344	445	6580	25 770	3.19	0.64
1c	352	440	5700	25 560	3.17	0.65
1d	357	457	6110	24 960	3.09	0.60
1e	342	447	6880	25 800	3.20	0.55
1f	345	434	5930	26 020	3.23	0.68
1g	347	427	5410	26 120	3.24	0.70
1h	344	437	6220	25 960	3.22	0.64
1i	324	401	5910	27 920	3.46	0.04
1j	314	403	7070	28 320	3.51	<0.01
2a	360	458	5940	24 810	3.08	0.64
3a	363	461	5860	24 620	3.05	0.62
4a	354	449	5980	25 260	3.13	0.62
5a	356	445	5620	25 280	3.13	0.63
6a	368	471	5940	24 200	3.00	0.61
7a	373	472	5620	24 000	2.98	0.60
8a	365	470	6120	24 340	3.02	0.60
9a	368	480	6340	24 000	2.98	0.57
10a	360	487	7240	24 160	2.99	0.39
10j	312	440	9324	27 390	3.40	0.28

[a] Data from reference 10. [b] Zero–zero transition energy; estimated based on $\Delta E_{00} = (E_{abs}(max) + E_{em}(max))/2$. [c] Fluorescence quantum yield; quinine sulfate as reference.

processes, all derivatives contain an unsubstituted benzene ring in the 5-position.[35]

The synthesis and photophysical data of compounds **1a–j** have been previously reported.[10] The remaining compounds **2a–10a** and **10j** used for this study were synthesized in the same fashion: aldol condensation of benzaldehyde with the corresponding fluoro acetophenone derivative yielded a chalcone intermediate, which was reacted with phenyl hydrazine to give the corresponding racemic triarylpyrazoline. Because we observed undesired nucleophilic substitution products with some fluoro acetophenones when using piperidine as catalyst, we performed the aldol condensation in aqueous ethanol using sodium hydroxide as base.

Steady-state absorption and emission spectroscopy

As pointed out in the introduction, the excited state energy of the fluorophore is one of the critical parameters that determines the PET kinetics. It can be estimated as the average of the absorption and emission maxima.[36] An overview of all measured photophysical data is provided with Table 3. All compounds were characterized in acetonitrile at 298 K.

With increasing electron withdrawing ability of the aryl ring attached to the 1-position of the pyrazoline ring (compounds **1a–1j**), a substantial shift of the absorption and emission bands to higher energy occurred. As a consequence, the excited state energy ΔE_{00} increased steadily from 24940 to 28320 cm^{-1}, spanning a total range of 3380 cm^{-1}. This observation is consistent with the decreasing degree of charge delocalization from the pyrazoline nitrogen lone pair towards the adjacent 3-aryl ring. Conversely, with increasing electron withdrawing ability of the aryl ring attached to the 3-position, a shift to lower energies is observed (compounds **1a–10a**). The overall change of the excited state energy of 780 cm^{-1} is in this case substantially smaller compared to the shift invoked by the same substituents attached to the 1-position. A graphical representation of the normalized UV–vis absorption and emission spectra reveals a uniform half-width distribution of all derivatives, indicating similar shapes for the ground and excited state potential energy wells (Fig. 2). The entire set of derivatives cover a tunable range of excited state energies of 4320 cm^{-1}, corresponding to about 0.54 eV.

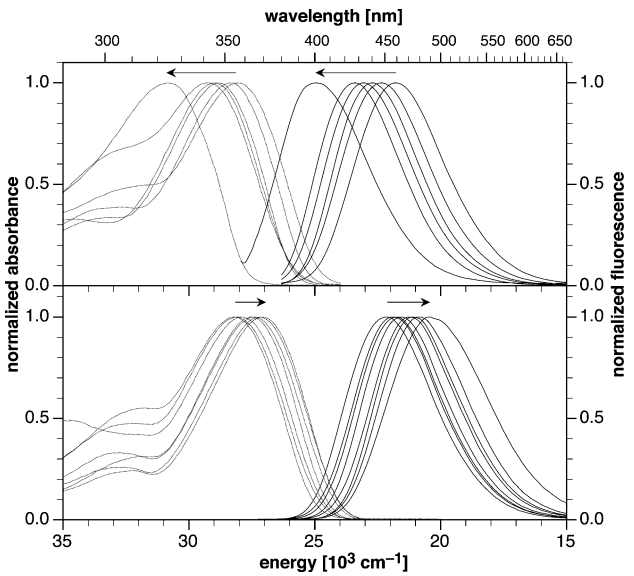

Fig. 2 Normalized absorption (dotted traces) and emission spectra (solid traces) of compounds **1a–j** (top) and **1a–10a** (bottom) in acetonitrile. The arrows indicate the direction of the band shift with increasing number of fluoro substituents.

Electrochemistry

The second critical parameter that governs the PET kinetics is the reduction potential of the fluorophore which may act as an

Table 4 Donor and acceptor reduction half-wave potentials for pyrazoline derivatives **1a–1j**[a], **2a–10a**, and **10j** in acetonitrile/0.1 M Bu_4NPF_6 *vs* $Fc^{+/0}$ (298K)[b]

Compd	$E_{1/2}(D^+/D)$/V	$E_{1/2}(A/A^-)$/V	Compd	$E_{1/2}(D^+/D)$/V	$E_{1/2}(A/A^-)$/V
1a	0.45	–2.79	**2a**	0.42	–2.71
1b	0.57	–2.78	**3a**	0.45	–2.66
1c	0.56	–2.76	**4a**	0.39	–2.85
1d	0.45	–2.77	**5a**	0.44	–2.70
1e	0.60	–2.75	**6a**	0.48	–2.55
1f	0.64	–2.70	**7a**	0.49	–2.53
1g	0.73	–2.71	**8a**	0.49	–2.54
1h	0.65	–2.69	**9a**	0.53	–2.36
1i	0.84	–2.72	**10a**	0.60	–2.23
1j	0.82	–2.66	**10j**	1.05	–2.23

[a] Data from reference 10. [b] Glassy carbon working electrode, $Ag/AgNO_3$ (10 mM) reference electrode, 100 mV/s scan rate.

electron acceptor in its excited state. To determine the variability of the ground state potentials $E(A/A^-)$ within the compound series that will be utilized for the LFER training set, we acquired cyclic voltammograms in acetonitrile with 0.1 M Bu_4NPF_6 as the electrolyte (Table 4).

As already observed for the excited state energies, fluoro substitution of the 1- vs. 3-aryl rings yielded quite divergent results. Substitution of the aryl ring in the 1-position affected the acceptor potential only to a small degree with an average potential centered around –2.74 ± 0.05 V (compounds **1a–1j**), while the potential varies by more than 0.6 V for compounds with fluoro substituents attached to the 3-aryl ring. Because in 1,3,5-triarylpyrazolines, the LUMO is more localized towards the 3-aryl ring, its energy is critically dependent on the nature of the substituents attached to this ring but to a much lesser degree on the adjacent ring. Consistent with a preferential location of the HOMO on the 1-aryl ring, the donor potentials vary significantly more for the compound series **1a–1j** compared to **1a–10a**.

Hammett LFER for the ET parameters ΔE_{00} and $E(A/A^-)$

Based on the initial assumption that the photophysical parameter P of interest is linearly correlated with the two computational Hammett constants $\sigma_1{}^c$ and $\sigma_2{}^c$ that capture the electron withdrawing properties of the 3- and 1-aryl rings, respectively, we can define a regression plane with the slopes s_1 and s_2 and the constant P_0.

$$P = P_0 + \sigma_1{}^c \cdot s_1 + \sigma_2{}^c \cdot s_2 \quad (4)$$

The acquired experimental data, specifically the excited state energy ΔE_{00} (Table 3) and the acceptor potential $E(A/A^-)$ (Table 4) of the pyrazolines **1a–1j**, **2a–10a**, and **10j**, served as the LFER training set to determine the regression parameters according to eqn (4). Derivative **10j**, which corresponds to the fully fluoro-substituted analog of derivative **1a**, served as an important anchor point to improve the reliability of the correlation. In addition, we performed a regression analysis for the sum of the two parameters, $\Delta E_{00} + E(A/A^-)$, which in combination with a donor potential $E(D^+/D)$ directly reflects the PET driving force $-\Delta G_{et}$ according to the Rehm-Weller eqn (1). In this context, this parameter can also be used to gauge the magnitude of the tunable range offered by the polyfluoro-substituted pyrazoline library. Table 5 provides an overview of the regression results for each of the three parameters, including the correlation coefficients as well as the average mean unsigned error (MUE). In addition, Fig. 3 illustrates the correlation for each compound series **1a–1j** and **1a–10a** as separate projections of the regression plane along a single Hammett variable, and thus shows how each photophysical parameter is influenced as a function of the two constants $\sigma_1{}^c$ and $\sigma_2{}^c$.

Table 5 Multi-linear regression analysis[a] for the Hammett LFER of the excited state energies and acceptor potentials of pyrazoline fluorophores **1a–1j**, **2a–10a**, and **10j**

Parameter (P)	P_0	s_1	s_2	r	MUE
ΔE_{00}/eV [b]	3.066	–0.073	0.336	0.959	0.035
$E(A/A^-)$/V [c]	–2.822	0.431	0.112	0.969	0.032
$-(\Delta E_{00}+E(A/A^-))$/eV	–0.244	–0.358	–0.448	0.986	0.028

[a] According to eqn (4). [b] Excited state energy (see Table 3) [c] Acceptor potential vs. $Fc^{+/0}$, 0.1 M Bu_4NPF_6 (see Table 4).

As already discussed in the previous paragraphs, the two aryl rings in the 1- and 3-positions influence the two parameters in distinctly different ways. The excited state energy increases with increasing electron withdrawing ability of the 1-aryl-ring (captured through $\sigma_2{}^c$), while the opposite trend is observed for the 3-aryl ring (Fig. 3a). Interestingly, the major outliers for this correlation all contain a para-fluoro substituent, whose effect is consistently overestimated by the computational Hammett constants σ^c. For example, when comparing unsubstituted phenyl with 4-fluorophenyl, σ^c increased from 0.03 to 0.2, while ΔE_{00} remained unchanged at 3.09 eV for the corresponding derivatives **1a** and **1d**. Similarly, ΔE_{00} minimally increased from 3.19 to 3.20 when a 4-fluoro substituent had been added to the 2-fluorophenyl group (derivative **1b** compared with **1e**), even though σ^c substantially increased from 0.28 to 0.44. In the case of derivative **1h**, which contains an additional 4-fluoro substituent compared to **1f**, ΔE_{00} even decreased from 3.23 to 3.22 eV, despite a significant increase of σ^c from 0.59 to 0.73. In all cases, the para-fluoro substituent is strongly π-donating and essentially cancels out its σ-accepting effect; however, this important resonance contribution is not captured by the computational Hammett constant.[30] The same resonance effect can also be seen for the pK_a's of 4-fluoro and 2,4,5-trifluorophenol, which are almost identical compared

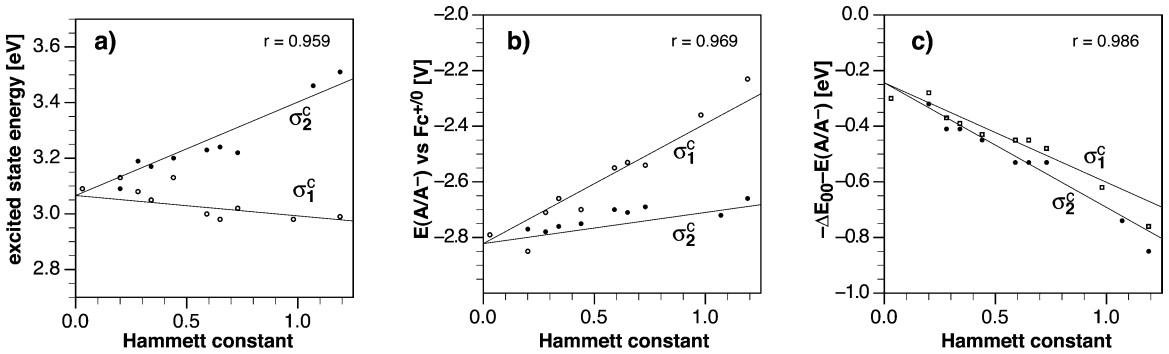

Fig. 3 Hammett linear free energy relationships for selected photophysical parameters of 1,3,5-triarylpyrazolines **1a–1j**, **2a–10a**, and **10j**. a) Correlation for the excited state energy ΔE_{00}, b) correlation for the acceptor potential $E(A/A^-)$, and c) correlation for the combined parameters ΔE_{00} and $E(A/A^-)$. Each graph shows two projections of the regression plane along the $\sigma_1{}^c$ and $\sigma_2{}^c$ Hammett constant coordinates.

to unsubstituted phenol and 2,5-difluorophenol, respectively (Table 1).

In the case of the acceptor potential $E(A/A^-)$, both aryl-rings yielded a similar trend; however, for a given Hammett constant the potential is pushed further upwards for the 3-aryl than the 1-aryl ring (Fig. 3b). As already noted above for the trends in ΔE_{00}, the major outliers are derivatives that contain a para-fluoro substituent. Finally, the combined excited state energies and acceptor potentials, $-(\Delta E_{00} + E(A/A^-))$, are similarly influenced by both Hammett constants, resulting in almost a superimposition of the two regression projections (Fig. 3c). The above opposing trends for ΔE_{00} *vs* $E(A/A^-)$ appear to cancel each other out to a large extent. This observation can be advantageous in the rational design of fluorescent PET sensors where tuning of the PET thermodynamics is of great importance. Specifically, Fig. 3c implies that the PET driving force can be tuned in two complementary ways, either by increasing the excited state energy ΔE_{00} combined with modest changes in reduction potentials $E(A/A^-)$, or by strongly pushing the acceptor potential $E(A/A^-)$ while slightly decreasing the excited state energy ΔE_{00}. As a consequence, it is possible to generate a pair of fluorophores offering identical PET driving forces, but exhibiting significantly different excited state energies and acceptor potentials. Each of the three regression analyses yielded acceptable correlation coefficients combined with a mean unsigned error (MUE) around 0.03 eV. The latter is comparable in size with the previous LFER, in which quantum chemical parameters derived for the entire fluorophore platform were utilized.[10] On the basis of the regression results, the overall tunable range of the PET driving force is 0.96 eV.

Evaluation of the Hammett LFER for polyfluoro-substituted pyrazolines

To test the performance of the LFER for predicting the photophysical parameters ΔE_{00} and $E(A/A^-)$ of derivatives that were not included in the training set, we synthesized and characterized an additional five pyrazolines with varying substituent combinations (compounds **3c**, **3g**, **7c**, **7i**, and **9g**). An overview of the compound numbering scheme, substituent key, as well as a list of predicted and experimental photophysical data are compiled in Table 6. All derivatives were brightly fluorescent with high quantum yields ranging between 0.66 to 0.73. The mean unsigned error (MUE) for the predicted excited state energies was somewhat larger compared to the MUE of the predicted reduction potentials; however, the combined parameters, $\Delta E_{00} + E(A/A^-)$, yielded an average MUE of less than 0.05 eV.

Fig. 4a illustrates the correlation results for the sum of the excited state energy and acceptor potential, $\Delta E_{00} + E(A/A^-)$, in the form of a 3D-plot. As pointed out above, in combination with a given donor potential $E(D^+/D)$, this combined parameter directly reflects the tunability of the PET driving force. The training set data points are plotted as black spheres, the regression plane is shown as a semi-transparent surface, and the test data set (which was not included in the regression analysis) is represented by red spheres. The plane visualizes the overall accessible dynamic range for adjusting the PET driving force within a library composed of all possible fluoro substituent combinations. The relative position of the test data points with regard to the regression plane is best visualized with a 2D-projection of the plane along the diagonal

Table 6 Predicted[a] and experimental data for pyrazoline derivatives **3c**, **3g**, **7c**, **7i**, and **9g** in acetonitrile (298 K)

Compd	R^1	R^2	$\sigma_1{}^c$	$\sigma_2{}^c$	ΔE_{00}/ eV[a,b]	$E(A/A^-)$[a,c]/V	$-\Delta E_{00} - E$ (A/A^-)[a]/eV	abs λ_{max}/nm	em λ_{max}/nm	ΔE_{00}/ eV[b]	$E(A/A^-)$/V[c]	$-\Delta E_{00} - E$ (A/A^-)/eV	Φ_F[d]
3c	3-F	3-F	0.34	0.34	3.16	−2.64	−0.52	358	449	3.11	−2.61	−0.50	0.66
3g	3-F	3,5-F_2	0.34	0.65	3.26	−2.60	−0.66	353	435	3.18	−2.56	−0.62	0.73
7c	3,5-F_2	3-F	0.65	0.34	3.13	−2.50	−0.63	363	459	3.06	−2.48	−0.58	0.66
7i	3,5-F_2	2,3,5,6-F_4	0.65	1.07	3.38	−2.42	−0.96	331	415	3.37	−2.45	−0.92	0.69
9g	2,3,4,5-F_4	3,5-F_2	0.98	0.65	3.21	−2.33	−0.89	356	451	3.12	−2.32	−0.80	0.69
MUE[e]					0.061	0.026	0.046						

[a] Predicted data according to eqn (4) using the regression parameters listed in Table 5. [b] Zero–zero transition energy; estimated based on $\Delta E_{00} = (E_{abs}(max)+E_{em}(max))/2$. [c] Acceptor potential vs. $Fc^{+/0}$, 0.1 M Bu_4NPF_6. [d] Fluorescence quantum yield (quinine sulfate as reference). [e] Mean unsigned error.

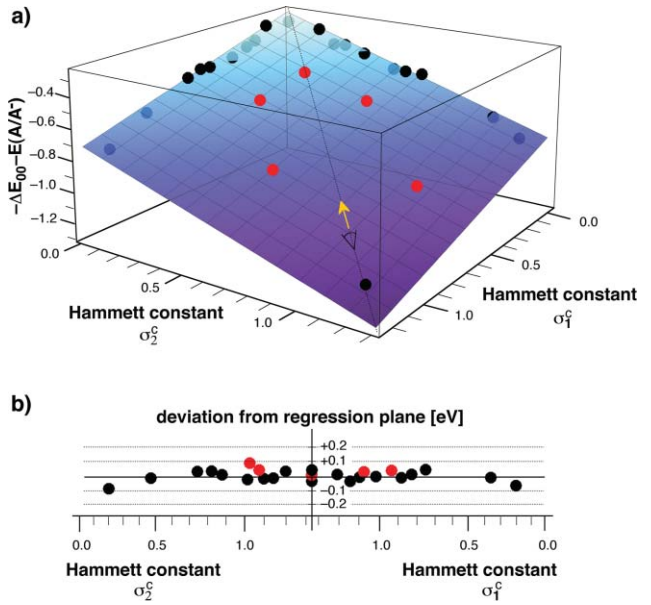

Fig. 4 Hammett LFER according to eqn (4) of the combined excited state energy ΔE_{00} and reduction potential $E(A/A^-)$ of pyrazolines **1a–j**, **2a–10a**, and **10j**. a) 3D representation of the training set data points (black; Table 3 and 4), the test data points (red, Table 6), and the regression plane (blue, Table 5). b) Projection of above regression plane along the diagonal vector shown in yellow.

vector shown in yellow (Fig. 4b). The plot reveals evenly spread data points for both the training set as well as for the test set without apparent systematic deviations. It is noteworthy that the maximum absorption and emission wavelengths of derivatives **3c** and **9g** coincide within 2 nm, while their reduction potentials differ by almost 0.3 V. In the context of tuning the PET thermodynamics for optimizing the contrast ratio of fluorescent probes,[10] the two derivatives would yield substantially different driving forces while offering essentially the same absorption and emission properties. Conversely, it would also be possible to tune the excited state energy without significantly altering the PET thermodynamics.

Conclusions

For a library composed of polyfluoro-substituted 1,3-diaryl-5-phenyl-pyrazoline fluorophores, two of the key parameters that govern the PET thermodynamics, the excited state energy ΔE_{00} and the acceptor potential $E(A/A^-)$, are altered in a systematic fashion. The observed trends of the two thermodynamic parameters were effectively captured through a multi-linear Hammett LFER using a set of independent substituent constants for each of the two aryl rings. Given the lack of experimental substituent constants for polyfluoro-substituted phenyl radicals, theoretically derived constants based on EPN values as local descriptors were employed. The LFER yielded comparable mean unsigned errors for the training set as well as the test set compounds. The prediction of the PET thermodynamic parameters is obviously limited to the experimental conditions utilized to calibrate the training set LFER. We also do not anticipate that the derived correlation is directly applicable to pyrazoline derivatives containing substituents other than fluorine. The contribution of resonance effects might greatly affect both the excited state energy and the acceptor potential of the fluorophore. Nevertheless, within the framework of polyfluoro-substituted pyrazolines, the outlined LFER approach should be well suited for designing and optimizing the performance and contrast ratio of cation-responsive fluorescent probes.

Experimental

Computational methods

All quantum chemical calculations were carried out with the QChem electronic structure calculation software.[37] Each of the fluoro-substituted benzene derivatives was energy minimized by DFT with the B3LYP hybrid[38,39] and Pople's 6-311+G(2d,2p) split valence basis set with added diffuse and polarization functions. To ensure a stationary point on the potential surface, all geometry-optimized structures were verified by a vibrational frequency analysis. The electrostatic potential at the nucleus of interest (EPN) was calculated using the implementation in QChem. A series of test calculations reproduced recent literature data and validated the application of eqn (3) as published.[30] Coordinates for all geometry optimized structures are provided with the supporting information.

Absorption and fluorescence spectroscopy

UV–vis absorption spectra were acquired at 25 °C with a Varian Cary Bio50 spectrometer with constant-temperature accessory. Emission spectra were recorded with a PTI fluorimeter. The fluorescence spectra were corrected for the spectral response of the detection system and for the spectral irradiance of the excitation source (via a calibrated photodiode). For all measurements the path length was 1 cm with a cell volume of 3.0 mL. Sample solutions were filtered through 0.45 μm Teflon membrane filters to remove interfering dust particles. Quantum yields were determined using quinine sulfate dihydrate in 1.0 N H_2SO_4 as a fluorescence standard ($\Phi_f = 0.54 \pm 0.05$).[40]

Cyclic voltammetry

The donor and acceptor potentials of the pyrazoline fluorophores were determined through cyclic voltammetry in acetonitrile containing 0.1 M Bu_4NPF_6 as an electrolyte with a CH-instruments potentiostat (model 600A). The samples were measured under an inert gas at a concentration of 3 mM in a single compartment cell with a glassy carbon working electrode, a Pt counter electrode, and a $Ag/AgNO_3$ (10 mM in 0.1 M Bu_4NPF_6/CH_3CN) nonaqueous reference electrode. All potentials were referenced to the ferrocenium/ferrocene couple ($Fc^{+/0}$) as an internal or external standard.

Materials and reagents

2-Fluorophenylhydrazine hydrochloride, 3-fluorophenylhydrazine hydrochloride, 4-fluorophenylhydrazine hydrochloride, 2,4-difluorophenylhydrazine, 2,5-difluorophenylhydrazine, 2,3,5,6-tetrafluorophenylhydrazine, pentafluorophenylhydrazine (Oakwood Products); 3,5-difluorophenylhydrazine hydrochloride (Aldrich). NMR: δ in ppm *vs* $SiMe_4$ (0 ppm, ^1H, 400 MHz). MS: selected peaks; m/z. Melting points are uncorrected. Flash chromatography (FC): Merck silica gel (70–230 mesh). TLC:

0.25 mm, Merck silica gel 60 F_{254}, visualizing at 254 nm or with 2% $KMnO_4$ solution.

Synthesis

General method A.

*Aldol condensation of acetophenone derivatives with benzaldehyde (chalcone derivatives **11–19**).* To a solution of sodium hydroxide (1.15 mmol) in water (1.3 ml) and ethanol (1.3 ml) was added benzaldehyde (2.6 mmol) and the corresponding fluoroacetophenone derivative (2.4 mmol). The reaction mixture was stirred at room temperature for 1–2 hr. After completion of the reaction (TLC, 5% EtOAc in hexane) the precipitated product was filtered off and washed with ethanol and hexane to yield the corresponding chalcone. In cases where the product did not precipitate, the reaction mixture was extracted with diethylether. The combined organic layers were dried over anhydrous sodium sulfate and concentrated under reduced pressure to afford the crude product, which was further purified by flash chromatography on silica gel.

General method B.

*Synthesis of racemic 1,3,5-triarylpyrazolines from chalcones and phenylhydrazine derivatives (derivatives **2a–10a**, **10j**, **3c**, **3g**, **7c**, **7i**, **9g**).* A solution of the corresponding phenylhydrazine derivative (1 mmol), chalcone (0.33 mmol), and 98% sulfuric acid (0.5 mmol) in 2.0 mL absolute ethanol was heated at reflux temperature for 8 hours. The reaction mixture was neutralized with saturated aq. $NaHCO_3$ and extracted twice with ethyl acetate. The combined organic phase was dried with anhydrous $MgSO_4$ and concentrated. The crude product was purified by flash chromatography and analytical purity was verified by reversed-phase HPLC (Varian ProStar system with UV detector, acetonitrile-water, gradient 20%–> 2% water).

3-(2-Fluorophenyl)-1,5-diphenyl-4,5-dihydro-1*H*-pyrazole (2a). Synthesized from chalcone **11** and phenylhydrazine (method B). Yield: 41%. M.p. 106–108 °C. ^{1}H NMR ($CDCl_3$, 400 MHz) δ 3.20 (ddd, J = 17.9, 7.4, 2.9 Hz, 1H), 3.88 (ddd, J = 17.9, 12.5, 2.9 Hz, 1H), 5.20 (dd, J = 12.5, 7.4 Hz, 1H), 6.72 (tt, J = 7.3, 1.2 Hz, 1H), 6.95–7.00 (m, 3H), 7.08–7.13 (m, 3H), 7.16–7.29 (m, 6H), 7.98 (td, J = 7.8, 1.8 Hz, 1H). ^{13}C NMR ($CDCl_3$, 100 MHz) δ 45.7 (d, J_{CF} = 7.6 Hz), 64.5 (d, 2.6 Hz), 113.4, 116.3 (d, J_{CF} = 22.3 Hz), 119.3, 120.8 (J_{CF} = 11.0 Hz), 124.2 (d, J_{CF} = 3.5 Hz), 125.8, 127.5, 128.3 (d, J_{CF} = 3.8 Hz), 128.9, 129.1, 130.0 (d, J_{CF} = 8.4 Hz), 142.5, 143.3 (d, J_{CF} = 2.7 Hz), 144.6, 160.4 (d, J_{CF} = 251.5 Hz). MS (70 eV) 316 (M^+, 56), 314 (100), 239 (25), 91 (27). EI HRMS m/z calcd for $[M]^+$ $C_{21}H_{17}FN_2$ 316.1376, found 316.1360.

3-(3-Fluorophenyl)-1,5-diphenyl-4,5-dihydro-1*H*-pyrazole (3a). Synthesized from chalcone **12** and phenylhydrazine (method B). Yield: 45%. M.p. 102–104 °C. ^{1}H NMR ($CDCl_3$, 400 MHz) δ 3.05 (dd, J = 17.1, 7.2 Hz, 1H), 3.75 (dd, J = 17.1, 12.5 Hz, 1H), 5.24 (dd, J = 12.5, 7.2 Hz, 1H), 6.73 (tt, J = 7.3, 1.1 Hz, 1H), 6.94 (tdd, J = 8.4, 2.6, 0.9 Hz, 1H), 6.98–7.14 (m, 2H), 7.17–7.29 (m, 2H), 7.17–7.29 (m, 6H), 7.36 (dt, J = 7.8, 1.1 Hz, 1H), 7.39 (ddd, J = 10.1, 2.5, 1.5 Hz, 1H). ^{13}C NMR ($CDCl_3$, 100 MHz) δ 43.3, 64.5, 112.3 (d, J_{CF} = 22.9 Hz), 113.4, 115.3 (d, J_{CF} = 21.5 Hz), 119.4, 121.3 (d, J_{CF} = 2.1 Hz), 125.8, 127.6, 128.9, 129.1, 130.0 (d, J_{CF} = 8.3 Hz), 134.9 (d, J_{CF} = 8.2 Hz), 142.2, 144.4, 145.4 (d, J_{CF} = 2.9 Hz), 162.9 (d, J_{CF} = 245.5 Hz). MS (70 eV) 316 (M^+, 100), 239 (60), 91 (56). EI HRMS m/z calcd for $[M]^+$ $C_{21}H_{17}FN_2$ 316.1376, found 316.1349.

3-(4-Fluorophenyl)-1,5-diphenyl-4,5-dihydro-1*H*-pyrazole (4a). Synthesized from chalcone **13** and phenylhydrazine (method B). Yield: 49%. M.p. 124–126 °C. ^{1}H NMR ($CDCl_3$, 400 MHz) δ 3.05 (dd, J = 17.0, 7.3 Hz, 1H), 3.76 (dd, J = 17.0, 12.4 Hz, 1H), 5.20 (dd, J = 12.4, 7.3 Hz, 1H), 6.71 (td, J = 7.3, 1.1 Hz, 1H), 6.97–7.03 (m, 4H), 7.08–7.13 (m, 2H), 7.17–7.21 (m, 2H), 7.24–7.29 (m, 4H), 7.60–7.65 (m, 1H). ^{13}C NMR ($CDCl_3$, 100 MHz) δ 43.6, 64.5, 113.3, 115.5 (d, J_{CF} = 21.7 Hz), 119.1, 125.8, 127.4 (d, J_{CF} = 8.2 Hz), 127.6, 128.8, 128.97 (d, J_{CF} = 3.2 Hz), 129.1, 142.4, 144.8, 145.7 (d, J_{CF} = 0.9 Hz), 162.9 (d, J_{CF} = 248.8 Hz). MS (70 eV) 316 (M^+, 100), 239 (55), 91 (55). EI HRMS m/z calcd for $[M]^+$ $C_{21}H_{17}FN_2$ 316.1376, found 316.1357.

3-(2,4-Difluorophenyl)-1,5-diphenyl-4,5-dihydro-1*H*-pyrazole (5a). Synthesized from chalcone **14** and phenylhydrazine (method B). Yield: 55%. M.p. 108–110 °C. ^{1}H NMR ($CDCl_3$, 400 MHz) δ 3.17 (ddd, J = 17.8, 7.5, 2.9 Hz, 1H), 3.85 (ddd, J = 17.8, 12.5, 2.9 Hz, 1H), 5.19 (dd, J = 12.5, 7.5 Hz, 1H), 6.70–6.76 (m, 2H), 6.83–6.88 (m, 1H), 6.96–6.99 (m, 2H), 7.08–7.13 (m, 2H), 7.17–7.30 (m, 5H), 7.97 (td, J = 8.8. 6.6 Hz, 1H). ^{13}C NMR ($CDCl_3$, 100 MHz) δ 45.5 (d, J_{CF} = 7.5 Hz), 64.4 (d, J_{CF} = 2.7 Hz), 104.4 (dd, J_{CF} = 25.8, 25.8 Hz), 111.9 (dd, J_{CF} = 21.6, 3.5 Hz), 113.4, 117.3 (dd, J_{CF} = 11.4, 3.9 Hz), 119.3, 125.8, 127.6, 128.9, 129.1, 129.4 (dd, J_{CF} = 9.4, 5.3 Hz), 142.3, 142.4 (dd, J_{CF} = 2.7, 1.6 Hz), 144.6, 160.4 (d, J_{CF} = 250.5, 11.6 Hz), 162.9 (d, J_{CF} = 248.3, 11.8 Hz). MS (70 eV) 334 (M^+, 100), 257 (65), 91 (54). EI HRMS m/z calcd for $[M]^+$ $C_{21}H_{16}F_2N_2$ 334.1282, found 334.1275.

3-(2,5-Difluorophenyl)-1,5-diphenyl-4,5-dihydro-1*H*-pyrazole (6a). Synthesized from chalcone **15** and phenylhydrazine (method B). Yield: 45%. M.p. 145–147 °C. ^{1}H NMR ($CDCl_3$, 400 MHz) δ 3.18 (ddd, J = 17.9, 7.4, 3.0 Hz, 1H), 3.86 (ddd, J = 17.9, 12.6, 3.0 Hz, 1H), 5.24 (dd, J = 12.6, 7.4 Hz, 1H), 6.74 (tt, J = 7.3, 1.1 Hz, 1H), 6.85–6.96 (m, 2H), 6.97–7.00 (m, 2H), 7.09–7.14 (m, 2H), 7.17–7.29 (m, 5H), 7.69 (ddd, J = 9.2, 6.0, 3.1 Hz, 1H). ^{13}C NMR ($CDCl_3$, 100 MHz) δ 45.3 (d, J_{CF} = 8.1 Hz), 64.6 (d, J_{CF} = 2.8 Hz), 113.5, 113.9 (dd, J_{CF} = 25.7, 4.3 Hz), 116.3 (dd, J_{CF} = 24.7, 8.6 Hz), 117.4 (dd, J_{CF} = 25.3, 8.6 Hz), 119.6, 122.1 (dd, J_{CF} = 13.8, 8.4 Hz), 125.8, 127.6, 128.9, 129.1, 142.0 (dd, J_{CF} = 2.6, 2.6 Hz), 142.2, 144.2, 156.3 (dd, J_{CF} = 248.8, 2.0 Hz), 158.6 (dd, J_{CF} = 242.0, 1.8 Hz). MS (70 eV) 334 (M^+, 100), 257 (65), 91 (55). EI HRMS m/z calcd for $[M]^+$ $C_{21}H_{16}F_2N_2$ 334.1282, found 334.1261.

3-(3,5-Difluorophenyl)-1,5-diphenyl-4,5-dihydro-1*H*-pyrazole (7a). Synthesized from chalcone **16** and phenylhydrazine (method B). Yield: 71%. M.p. 166–168 °C. ^{1}H NMR ($CDCl_3$, 400 MHz) δ 3.01 (dd, J = 17.1, 7.2 Hz, 1H), 3.72 (dd, J = 17.1, 12.6 Hz, 1H), 5.27 (dd, J = 12.6, 7.2 Hz, 1H), 6.68 (tt, J = 8.8, 2.3 Hz, 1H), 6.75 (tt, J = 7.2, 1.0 Hz, 1H), 6.98–7.00 (m, 2H), 7.09–7.16 (m, 3H), 7.18–7.29 (m, 6H). ^{13}C NMR ($CDCl_3$ 100 MHz) δ 43.1, 64.7, 103.5 (t, J_{CF} = 25.8 Hz), 108.3 (dd, J_{CF} = 19.2, 7.5 Hz), 113.5, 119.7, 125.7, 127.8, 129.0, 129.2, 136.0 (t, J_{CF} = 10.0 Hz), 141.9, 144.0, 144.3 (t, J_{CF} = 3.6 Hz), 163.1 (dd, J_{CF} = 247.9, 12.9 Hz). MS (70 eV) 334 (M^+, 100), 257 (60), 91 (55). EI HRMS m/z calcd for $[M]^+$ $C_{21}H_{16}F_2N_2$ 334.1282, found 334.1287.

3-(2,4,5-Trifluorophenyl)-1,5-diphenyl-4,5-dihydro-1*H*-pyrazole (8a). Synthesized from chalcone **17** and phenylhydrazine (method B). Yield: 40%. M.p. 124–126 °C. ^{1}H NMR ($CDCl_3$, 400 MHz) δ 3.15 (ddd, J = 17.9, 7.5, 3.0 Hz, 1H), 3.83 (ddd, J = 17.9, 12.6, 3.0 Hz, 1H), 5.22 (dd, J = 12.6, 7.4 Hz, 1H), 6.74 (tt, J = 7.3, 1.1 Hz, 1H), 6.84 (td, J = 10.2, 6.5 Hz, 1H), 6.95–6.98 (m, 2H), 7.08–7.14 (m, 2H), 7.17–7.22 (m, 3H), 7.25–7.29 (m, 2H), 7.83 (ddd, 11.2, 9.0, 6.9 Hz, 1H). ^{13}C NMR ($CDCl_3$, 100 MHz) δ 45.3, (d, J_{CF} = 7.9 Hz), 64.7 (d, J_{CF} = 2.8 Hz), 106.1 (dd, J_{CF} = 28.5, 21.1 Hz), 113.5, 115.4 (dd, J_{CF} = 20.7, 5.4 Hz), 117.5 (m), 119.7, 125.8, 127.7, 129.0, 129.2, 141.3 (m), 142.1, 144.2, 147.0 (ddd, J_{CF} = 245.0, 12.9, 3.0 Hz), 149.9 (ddd, J_{CF} = 254.1, 14.9, 12.2 Hz), 155.3 (ddd, J_{CF} = 248.3, 9.2, 2.1 Hz). MS (70 eV) 352 (M^+, 100), 275 (50), 91 (48), 77 (28). EI HRMS m/z calcd for $[M]^+$ $C_{21}H_{15}F_3N_2$ 352.1187, found 352.1182.

3-(2,3,4,5-Tetrafluorophenyl)-1,5-diphenyl-4,5-dihydro-1*H*-pyrazole (9a). Synthesized from chalcone **18** and phenylhydrazine (method B). Yield: 44%. M.p. 126–128 °C. ^{1}H NMR ($CDCl_3$, 400 MHz) δ 3.16 (ddd, J = 17.9, 7.4, 2.9 Hz, 1H), 3.84 (ddd, J = 17.9, 12.6, 2.9 Hz, 1H), 5.27 (dd, J = 12.6, 7.4 Hz, 1H), 6.76 (tt, J = 7.3, 1.0 Hz, 1H), 6.96–6.99 (m, 2H), 7.09–7.14 (m, 2H), 7.18–7.22 (m, 3H), 7.25–7.29 (m, 2H), 7.61 (dddd, J = 11.0, 8.5, 6.4, 2.5 Hz, 1H). ^{13}C NMR ($CDCl_3$, 100 MHz) δ 44.9 (d, J_{CF} = 7.4 Hz), 64.8 (d, J_{CF} = 2.0 Hz), 108.4 (ddd, J_{CF} = 20.9, 2.8, 2.8 Hz), 113.6, 117.4 (m), 120.0, 125.7, 127.8, 128.9, 129.2, 140.1 (dd, J_{CF} = 243.5, 19.2 Hz), 140.2, 141.1 (dddd, J_{CF} = 250.0, 12.4, 10.3, 4.4 Hz), 141.8, 143.8, 145.5 (ddd, J_{CF} = 252.0, 11.6, 3.0 Hz), 147.1 (dddd, J_{CF} = 246.9, 10.6, 2.5, 2.5 Hz). MS (70 eV) 370 (M^+, 100), 293 (46), 91 (35), 77 (19). EI HRMS m/z calcd for $[M]^+$ $C_{21}H_{14}F_4N_2$ 370.1093, found 370.1073.

3-(Perfluorophenyl)-1,5-diphenyl-4,5-dihydro-1*H*-pyrazole (10a). Synthesized from chalcone **19** and phenylhydrazine (method B). Yield: 90%. M.p. 138–140 °C. ^{1}H NMR ($CDCl_3$, 400 MHz) δ 3.14 (dd, J = 17.7, 7.3 Hz, 1H), 3.83 (dd, J = 17.6, 12.6 Hz, 1H), 5.22 (dd, J = 17.6, 12.6 Hz, 1H), 5.22 (dd, J = 12.6, 7.3 Hz, 1H), 6.5 (t, J = 7.3 Hz, 1H), 6.97 (dd, J = 8.8, 1.0 Hz, 2H), 7.08–7.12 (m, 2H), 7.16–7.21 (m, 3H), 7.24–7.28 (m, 2H). ^{13}C NMR ($CDCl_3$, 100 MHz) δ 45.9 (t, J_{CF} = 4.3 Hz), 63.8, 109.0 (td, J_{CF} = 13.6, 4.1 Hz), 113.7, 120.2, 125.7, 127.8, 128.9, 129.2, 135.7 (m), 137.9 (dm, J_{CF} = 251.6 Hz), 140.2 (dm, J_{CF} = 251.3 Hz), 141.5, 143.7, 144.7 (dm, J_{CF} = 254.6 Hz). MS (70 eV) 388 (M^+, 100), 311 (45), 91 (36), 77 (25). EI HRMS m/z calcd for $[M]^+$ $C_{21}H_{13}F_5N_2$ 388.0999, found 388.1000.

1,3-Bis(perfluorophenyl)-5-phenyl-4,5-dihydro-1*H*-pyrazole (10j). Synthesized from chalcone **19** and perfluorophenylhydrazine (method B). Yield: 3%. M.p. 83–85 °C. ^{1}H NMR ($CDCl_3$, 400 MHz) δ 3.34 (dd, J = 17.6, 8.9 Hz, 1H), 3.76 (dd, 17.6, 11.5 Hz, 1H), 5.33 (dd, 11.5, 8.9 Hz, 1H), 7.19–7.25 (m, 5H). ^{13}C NMR ($CDCl_3$ 100 MHz) δ 45.1 (t, J_{CF} = 3.9 Hz), 68.0, 108.3 (td, J_{CF} = 14.2, 4.1 Hz), 119.4 (td, J_{CF} = 11.9, 3.8 Hz), 126.6, 128.8, 129.0, 137.8 (dm, J_{CF} = 250.4 Hz), 137.9 (dm, J_{CF} = 251.2 hz), 138.7 (dtt, J_{CF} = 252.0, 13.7, 4.5 Hz), 139.1, 139.5 (m), 141.1 (dtt, J_{CF} = 252.0, 13.7, 4.5 Hz), 141.1 (dtt, J_{CF} = 256.8, 13.6, 4.7 Hz), 145.1 (dm, J_{CF} = 254.6 Hz). MS (70 eV) 478 (M+, 100), 401 (30), 374 (20), 296 (72), 181 (50), 103 (25), 77 (23). EI HRMS m/z calcd for $[M]^+$ $C_{21}H_8F_{10}N_2$ 478.0528, found 478.0511.

1,3-Bis(3-fluorophenyl)-5-phenyl-4,5-dihydro-1*H*-pyrazole (3c). Synthesized from chalcone **12** and 3-fluorophenylhydrazine (method B). Yield: 41%. M.p. 145–147 °C. ^{1}H NMR ($CDCl_3$, 400 MHz) δ 3.05 (dd, J = 17.2, 6.9 Hz, 1H), 3.76 (dd, J = 17.2, 12.4 Hz, 1H), 5.21 (dd, J = 12.4, 6.9 Hz, 1H), 6.40 (td, J = 8.3, 1.8 Hz, 1H), 6.64 (dd, J = 8.3, 1.5 Hz, 1H), 6.79 (dt, J = 11.8, 2.3 Hz, 1H), 6.96 (tdd, J = 8.3, 2.5, 0.9 Hz, 1H), 7.01 (td, J = 8.2, 6.7 Hz, 1H), 7.18–7.29 (m, 6H), 7.35–7.40 (m, 2H). ^{13}C NMR ($CDCl_3$, 100 MHz) δ 43.5, 64.4, 100.8 (d, J_{CF} = 26.9 Hz), 105.8 (d, J_{CF} = 21.6 Hz), 108.8 (d, J_{CF} = 2.3 Hz), 112.4 (d, J_{CF} = 22.9 Hz), 115.6 (d, J_{CF} = 21.5 Hz), 121.5 (d, J_{CF} = 2.8 Hz), 125.7, 127.8, 129.3, 130.0 (d, J_{CF} = 9.9 Hz), 130.1 (d, J_{CF} = 8.3 Hz), 134.6 (d, J_{CF} = 8.3 Hz), 141.7, 145.9 (d, J_{CF} = 10.8 Hz), 146.3 (d, J_{CF} = 3.1 Hz), 162.9 (d, 245.7 Hz), 163.6 (d, J_{CF} = 242.7 Hz). MS (70 eV) 334 (M^+, 100), 257 (40), 230 (12), 109 (50), 95 (18). EI HRMS m/z calcd for $[M]^+$ $C_{21}H_{16}F_2N_2$ 334.1282, found 334.1265.

1-(3,5-Difluorophenyl)-3-(3-fluorophenyl)-5-phenyl-4,5-dihydro-1*H*-pyrazole (3g). Synthesized from chalcone **12** and 3,5-difluorophenylhydrazine (method B). Yield: 33%. M.p. 164–166 °C. ^{1}H NMR ($CDCl_3$, 400 MHz) δ 3.07 (dd, J = 17.3, 6.6 Hz, 1H), 3.78 (dd, J = 17.3, 12.4 Hz, 1H), 5.18 (dd, 12.4, 6.6 Hz, 1H), 6.14 (tt, J = 9.1, 2.3 Hz, 1H), 6.44–6.51 (m, 2H), 6.98 (tdd, J = 8.3, 2.5, 0.9 Hz, 1H), 7.18–7.31 (m, 6H), 7.35–7.40 (m, 2H). ^{13}C NMR ($CDCl_3$, 100 MHz) δ 43.6, 64.3, 94.2 (t, J_{CF} = 26.4 Hz), 96.4 (dd, J_{CF} = 20.8, 9.2 Hz), 112.6 (d, J_{CF} = 22.9 Hz), 116.0 (d, J_{CF} = 21.5 Hz), 121.7 (d, J_{CF} = 2.5 Hz), 125.6, 128.1, 129.4, 130.1 (d, J_{CF} = 8.3 Hz), 134.2 (d, J_{CF} = 8.3 Hz), 141.2, 146.2 (t, J_{CF} = 13.7 Hz), 147.2 (d, J_{CF} = 3.1 Hz), 162.9 (d, J_{CF} = 245.8 hz), 163.6 (dd, J_{CF} = 244.1, 15.7 Hz). MS (70 eV) 352 (M^+, 100), 275 (36), 248 (13), 127 (30). EI HRMS m/z calcd for $[M]^+$ $C_{21}H_{15}F_3N_2$ 352.1187, found 352.1170.

3-(3,5-Difluorophenyl)-1-(3-fluorophenyl)-5-phenyl-4,5-dihydro-1*H*-pyrazole (7c). Synthesized from chalcone **16** and 3-fluorophenylhydrazine (method B). Yield: 42%. M.p. 188–190 °C. ^{1}H NMR ($CDCl_3$, 400 MHz) δ 3.03 (dd, J = 17.1, 6.8 Hz, 1H), 3.73 (dd, J = 17.1, 12.6 Hz, 1H), 5.25 (dd, J = 12.6, 6.8 Hz, 1H), 6.42 (td, J = 8.3, 2.4 Hz, 1H), 6.65 (dd, J = 8.3, 2.1 Hz, 1H), 6.70 (tt, J = 8.8, 2.2 Hz, 1H), 6.78 (dt, J = 11.7, 2.1 Hz, 1H), 7.02 (td, J = 7.9, 6.9 Hz, 1H), 7.11–7.23 (m, 5H), 7.26–7.30 (m, 2H). ^{13}C NMR ($CDCl_3$, 100 MHz) δ 43.3, 64.6, 100.9 (d, J_{CF} = 26.9 Hz), 103.9 (t, J_{CF} = 25.8 Hz), 106.2 (d, J_{CF} = 21.5 Hz), 108.3, 108.5 (d, J_{CF} = 11.7 Hz), 108.6, 108.9 (d, J_{CF} = 2.5 Hz), 125.6, 128.0, 129.3, 130.1 (d, J_{CF} = 9.9 Hz), 135.6 (t, J_{CF} = 9.9 Hz), 141.4, 145.2 (t, J_{CF} = 3.5 Hz), 145.6 (d, J_{CF} = 10.8 Hz), 163.1 (dd, J_{CF} = 248.1, 12.9 Hz), 163.5 (d, J_{CF} = 243.0 Hz). MS (70 eV) 352 (M^+, 100), 275 (38), 109 (28). EI HRMS m/z calcd for $[M]^+$ $C_{21}H_{15}F_3N_2$ 352.1187, found 352.1184.

3-(3,5-Difluorophenyl)-5-phenyl-1-(2,3,5,6-tetrafluorophenyl)-4,5-dihydro-1*H*-pyrazole (7i). Synthesized from chalcone **16** and 2,3,5,6-tetrafluorophenylhydrazine (method B). Yield: 72%. M.p. 112–114 °C. ^{1}H NMR ($CDCl_3$, 400 MHz) δ 3.19 (dd, J = 17.0, 7.5 Hz, 1H), 3.66 (dd, J = 17.0, 12.0 Hz, 1H), 5.50 (dd, J = 12.0, 7.5 Hz), 6.62 (tt, J = 9.8, 7.1 Hz, 1H), 6.73 (tt, J = 8.7, 2.2 Hz, 1H), 7.11–7.33 (m, 7H). ^{13}C NMR ($CDCl_3$, 100 MHz) δ 42.2, 67.8 (t, J_{CF} = 3.3 Hz), 100.5 (t, J_{CF} = 23.1 Hz), 104.2 (t, J_{CF} = 25.5 Hz), 108.6 (dd, J_{CF} = 19.2, 7.4 Hz), 124.2 (tt, J_{CF} = 10.9, 2.9 Hz), 126.4, 128.5, 129.0, 135.3 (t, J_{CF} = 9.9 Hz), 140.0, 141.3 (dtt, J_{CF} = 249.1,

14.9, 4.0 Hz), 146.2 (dtd, J_{CF} = 246.5, 13.0, 3.9 Hz), 147.3 (t, J_{CF} = 3.8 Hz), 163.1 (dd, J_{CF} = 248.5, 12.9 Hz). MS (70 eV) 406 (M^+, 100), 329 (28), 242 (34), 163 (39). EI HRMS *m/z* calcd for $[M]^+$ $C_{21}H_{12}F_6N_2$ 406.0905, found 406.0896.

1-(3,5-Difluorophenyl)-5-phenyl-3-(2,3,4,5-tetrafluorophenyl)-4,5-dihydro-1*H*-pyrazole (9g). Synthesized from chalcone **18** and 3,5-difluorophenylhydrazine (method B). Yield: 43%. M.p. 159–161°C. ^{1}H NMR ($CDCl_3$, 400 MHz) δ 3.19 (ddd, *J* = 18.0, 6.7, 2.8 Hz, 1H), 3.87 (ddd, *J* = 18.0, 12.5, 2.8 Hz, 1H), 5.21 (dd, *J* = 12.5, 6.7 Hz, 1H), 6.17 (tt, *J* = 9.0, 2.3 Hz, 1H), 6.42–6.49 (m, 2H), 7.15–7.19 (m, 2H), 7.24 (tt, *J* = 7.2, 2.8 Hz, 1H), 7.29 (tt, *J* = 7.5, 1.5 Hz, 2H), 7.60 (dddd, *J* = 11.4, 8.6, 6.4, 2.6 Hz, 1H). ^{13}C NMR ($CDCl_3$, 100 MHz) δ 45.2 (d, J_{CF} = 7.6 Hz), 64.5 (d, J_{CF} = 2.7 Hz), 94.8 (t, J_{CF} = 52.3 Hz), 96.7 (dd, J_{CF} = 21.1, 9.3 Hz), 108.6 (dt, J_{CF} = 20.8, 3.4 Hz), 116.7 (m), 125.5, 128.2, 129.5, 140.6 (dddd, J_{CF} = 256.9, 17.1, 12.5, 2.8 Hz), 140.8, 141.1 (dddd, J_{CF} = 252.3, 16.5, 12.4, 4.0 Hz), 142.1 (t, J_{CF} = 2.9 Hz), 145.7 (t, J_{CF} = 13.4 Hz), 145.8 (ddd, J_{CF} = 253.3, 12.0, 3.3 Hz), 147.2 (ddt, J_{CF} = 247.2, 10.3, 3.0 Hz), 163.6 (dd, J_{CF} = 244.7, 15.4 Hz). MS (70 eV) 406 (M^+, 100), 329 (43), 127 (25). EI HRMS *m/z* calcd for $[M]^+$ $C_{21}H_{12}F_6N_2$ 406.0905, found 406.0900.

(*E*)-1-(2-Fluorophenyl)-3-phenylprop-2-en-1-one (11). Synthesized from 2-fluoroacetophenone (method A). Yield: 82%. Yellow oil. ^{1}H NMR ($CDCl_3$, 400 MHz) δ 7.09 (ddd, *J* = 10.8, 8.3, 1.0 Hz, 1H), 7.19 (td, *J* = 7.6, 1.0 Hz, 1H), 7.29–7.35 (m, 4H), 7.45 (dddd, *J* = 8.3, 7.3, 5.1, 1.9 Hz, 1H), 7.52–7.56 (m, 2H), 7.67 (dd, *J* = 15.8, 1.8 Hz, 1H), 7.74 (td, *J* = 7.5, 1.9 Hz, 1H). ^{13}C NMR ($CDCl_3$, 100 MHz) δ 116.3 (d, J_{CF} = 23.1 Hz), 124.3 (d, J_{CF} = 3.3 Hz), 125.4 (d, J_{CF} = 6.5 Hz), 126.9 (d, J_{CF} = 13.1 Hz), 128.4, 128.7, 130.5, 130.8 (d, J_{CF} = 2.5 Hz), 133.7 (J_{CF} = 8.7 Hz), 134.4, 144.6, 161.0 (d, J_{CF} = 253 Hz), 188.7. MS (70 eV) 226 (M^+, 78), 225 (100), 197 (20, 131 (36), 103 (34), 95 (20), 77 (22). EI HRMS *m/z* calcd for $[M]^+$ $C_{15}H_{11}FO$ 226.0794, found 226.0801.

(*E*)-1-(3-Fluorophenyl)-3-phenylprop-2-en-1-one (12). Synthesized from 3-fluoroacetophenone (method A). Yield: 81%. M.p. 57–59 °C. ^{1}H NMR ($CDCl_3$, 400 MHz) δ 7.29 (tdd, *J* = 8.3, 2.6, 0.9 Hz, 1H), 7.41–7.47 (m, 3H), 7.48 (d, *J* = 15.7 Hz, 1H), 7.49 (td, *J* = 8.0, 5.5 Hz, 1H), 7.63–7.67 (m, 2H), 7.71 (ddd, *J* = 9.4, 2.6, 1.5 Hz, 1H), 7.79–7.86 (m, 2H). ^{13}C NMR ($CDCl_3$, 100 MHz) δ 114.8 (d, J_{CF} = 22.3 Hz), 119.3 (d, J_{CF} = 21.4 Hz), 120.9, 123.8, 128.2, 128.6, 129.9 (d, J_{CF} = 7.6 Hz), 130.4 (d, J_{CF} = 4.0 Hz), 134.2, 139.8 (d, J_{CF} = 6.1 Hz), 144.9, 162.4 (d, J_{CF} = 247.7 Hz), 188.3. MS (70 eV) 226 (M^+, 92), 225 (100), 197 (14), 131 (39), 103 (32), 95 (25). EI HRMS *m/z* calcd for $[M]^+$ $C_{15}H_{11}FO$ 226.0794, found 226.0789.

(*E*)-1-(4-Fluorophenyl)-3-phenylprop-2-en-1-one (13). Synthesized from 4-fluoroacetophenone (method A). Yield: 65%. M.p. 77–79 °C. ^{1}H NMR ($CDCl_3$, 400 MHz) δ 7.19 (t, *J* = 8.7 Hz, 2H), 7.41–7.46 (m, 3H), 7.51 (d, *J* = 15.7 Hz, 1H), 7.63–7.67 (m, 2H), 7.82 (d, *J* = 15.7 Hz, 1H), 8.04–8.09 (m, 2H). ^{13}C NMR ($CDCl_3$, 100 MHz) δ 115.5 (d, J_{CF} = 21.9 Hz), 121.3, 128.3, 128.3, 128.8, 130.5, 130.9 (d, J_{CF} = 9.2 Hz), 134.3 (d, J_{CF} = 2.8 Hz), 134.6, 144.7, 165.4 (d, J_{CF} = 254.4 Hz), 188.5. MS (70 eV) 226 (M^+, 91), 197 (15), 123 (33), 95 (30), 77 (18). EI HRMS *m/z* calcd for $[M]^+$ $C_{15}H_{11}FO$ 226.0794, found 226.0787.

(*E*)-1-(2,4-Difluorophenyl)-3-phenylprop-2-en-1-one (14). Synthesized from 2,4-difluoroacetophenone (method A). Yield: 76%. M.p. 55–57 °C. ^{1}H NMR ($CDCl_3$, 400 MHz) δ 6.91 (ddd, *J* = 10.9, 8.7, 2.4 Hz, 1H), 7.00 (tdd, *J* = 7.7, 2.4, 0.8 Hz, 1H), 7.37–7.44 (m, 4H), 7.61–7.64 (m, 2H), 7.78 (dd, *J* = 15.7, 1.9 Hz, 1H), 7.90 (td, *J* = 8.6, 6.6 Hz, 1H). ^{13}C NMR ($CDCl_3$, 100 MHz) δ 104.3 (dd, J_{CF} = 27.2, 25.8 Hz), 111.7 (dd, J_{CF} = 21.4, 3.3 Hz), 123.1 (dd, J_{CF} = 13.1, 3.5 Hz), 124.6 (d, J_{CF} = 7.5 Hz), 128.2, 128.5, 130.3, 132.6 (dd, J_{CF} = 10.3, 4.1 Hz), 134.2, 144.4, 161.5 (dd, J_{CF} = 255.9, 12.6 Hz), 164.9 (dd, J_{CF} = 255.8, 12.2 Hz), 186.3 (d, J_{CF} = 3.4 Hz). MS (70 eV) 244 (M^+, 86), 243 (100), 141 (37), 103 (34), 77 (17). EI HRMS *m/z* calcd for $[M]^+$ $C_{15}H_{10}F_2O$ 244.0700, found 244.0692.

(*E*)-1-(2,5-Difluorophenyl)-3-phenylprop-2-en-1-one (15). Synthesized from 2,5-difluoroacetophenone (method A). Yield: 81%. M.p. 41–43 °C. ^{1}H NMR ($CDCl_3$, 400 MHz) δ 7.12–7.25 (m, 2H), 7.36–7.44 (m, 4H), 7.52 (ddd, *J* = 8.5, 5.4, 3.2 Hz, 1H), 7.61–7.64 (m, 2H), 7.77 (dd, *J* = 15.8, 1.6 Hz, 1H). ^{13}C NMR ($CDCl_3$, 100 MHz) δ 116.5 (dd, J_{CF} = 25.1, 3.1 Hz), 117.6 (dd, J_{CF} = 26.6, 7.9 Hz), 120.1 (dd, J_{CF} = 24.5, 9.2 Hz), 124.3 (d, J_{CF} = 7.5 Hz), 127.6 (dd, J_{CF} = 15.8, 6. 3 Hz), 128.3, 128.5, 130.5, 134.0, 144.9, 156.8 (dd, J_{CF} = 248.9, 1.6 Hz), 158.2 (d, J_{CF} = 243. 1.6 Hz), 186.5 (d, J_{CF} = 2.2 Hz). MS (70 eV) 244 (M^+, 92), 243 (100), 141 (25), 131 (36), 77 (20). EI HRMS *m/z* calcd for $[M]^+$ $C_{15}H_{10}F_2O$ 244.0700, found 244.0698.

(*E*)-1-(3,5-Difluorophenyl)-3-phenylprop-2-en-1-one (16). Synthesized from 3,5-difluoroacetophenone (method A). Yield: 67%. M.p. 73–75 °C. ^{1}H NMR ($CDCl_3$, 400 MHz) δ 7.04 (tt, *J* = 8.4, 2.3 Hz, 1H), 7.41 (d, 15.7 Hz, 1H), 7.42–7.46 (m, 3H), 7.49–7.55 (m, 2H), 7.63–7.68 (m, 2H), 7.85 (d, 15.7 Hz, 1H). ^{13}C NMR ($CDCl_3$, 100 MHz) δ 107.7 (t, J_{CF} = 25.3 Hz), 111.1 (dd, J_{CF} = 18.6, 7.1 Hz), 120.4, 128.4, 128.8, 130.8, 134.2, 140.9 (t, J_{CF} = 7.5 Hz), 145.9, 162.8 (dd, J_{CF} = 250.9, 12.0 Hz), 187.1 (t, J_{CF} = 2.4 Hz). MS (70 eV) 245 ((M + H)$^+$, 100), 141 (70), 113 (34), 77 (10). EI HRMS *m/z* calcd for $[M]^+$ $C_{15}H_{10}F_2O$ 244.0700, found 244.0701.

(*E*)-1-(2,4,5-Trifluorophenyl)-3-phenylprop-2-en-1-one (17). Synthesized from 2,4,5-trifluoroacetophenone (method A). Yield: 58%. M.p. 74–76 °C. ^{1}H NMR ($CDCl_3$, 400 MHz) δ 7.05 (td, *J* = 9.8, 6.1 Hz, 1H), 7.39 (dd, *J* = 15.7, 3.0 Hz, 1H), 7.40–7.45 (m, 3H), 7.61–7.66 (m, 2H), 7.73 (ddd, *J* = 10.3, 8.9, 6.5 Hz, 1H), 7.81 (dd, *J* = 15.7, 2.1 Hz, 1H). ^{13}C NMR ($CDCl_3$, 100 MHz) δ 106.5 (dd, J_{CF} = 29.9, 21.2 Hz), 118.8 (ddd, J_{CF} = 20.1, 4.5, 2.2 Hz), 123.2 (dt, J_{CF} = 15.6, 3.9 Hz), 124.3 (d, J_{CF} = 8.3 Hz), 128.6, 128.9, 130.9, 134.3, 145.5 (d, J_{CF} = 1.1 Hz), 147.0 (ddd, J_{CF} = 247.7, 12.7, 3.5 Hz), 152.7 (ddd, J_{CF} = 258.7, 14.6, 12.6 Hz), 156.8 (ddd, J_{CF} = 250.4, 9.9, 2.3 Hz), 185.6 (d, J_{CF} = 3.8 Hz). MS (70 eV) 262 (M^+, 80), 260 (100), 159 (25), 131 (30), 103 (25), 77 (18). EI HRMS *m/z* calcd for $[M]^+$ $C_{15}H_9F_3O$ 262.0605, found 262.0651.

(*E*)-1-(2,3,4,5-Tetrafluorophenyl)-3-phenylprop-2-en-1-one (18). Synthesized from 2,3,4,5-tetrafluoroacetophenone (method A). Yield: 82%. M.p. 122–124 °C. ^{1}H NMR ($CDCl_3$, 400 MHz) δ 7.36 (dd, *J* = 15.7, 3.1 Hz, 1H), 7.41–7.47 (m, 3H), 7.53 (dddd, *J* = 10.3, 8.2, 5.9, 2.5 Hz, 1H), 7.61–7.65 (m, 2H), 7.82 (dd, *J* = 15.7, 2.0 Hz, 1H). ^{13}C NMR ($CDCl_3$, 100 MHz) δ 111.9 (dt, J_{CF} = 20.3, 3.0 Hz), 122.6 (m), 124.0 (d, J_{CF} = 7.5 Hz), 128.8, 129.0, 131.3,

134.1, 140.9 (dddd, $J_{CF} = 255.8, 17.9, 12.4, 3.3$ Hz), 143.1 (dddd, $J_{CF} = 244.8, 16.1, 12.5, 3.8$ Hz), 146.5, 146.9 (dddd, $J_{CF} = 252.3, 11.3, 3.4, 1.3$ Hz), 147.2 (dddd, $J_{CF} = 250.4, 10.3, 3.3, 1.8$ Hz), 184.9. MS (70 eV) 280 (M^+, 80), 279 (100), 177 (15), 131 (16), 103 (20), 77 (16). EI HRMS m/z calcd for $[M]^+$ $C_{15}H_8F_4O$ 280.0511, found 280.0514.

(*E*)-1-(Perfluorophenyl)-3-phenylprop-2-en-1-one (19). Synthesized from 2,3,4,5,6-pentafluoroacetophenone (method A). Yield: 91%. M.p. 74–76 °C. ^{1}H NMR ($CDCl_3$, 400 MHz) δ 7.04 (dt, $J =$ 16.0, 1.3 Hz, 1H), 7.41–7.49 (m, 3H), 7.53 (d, $J = 16.0$ Hz, 1H), 7.57–7.59 (m, 2H). ^{13}C NMR ($CDCl_3$, 100 MHz) δ 114.5 (tm, $J_{CF} = 21.2$ Hz), 126.0, 128.8, 129.1, 131.6, 133.5, 137.6 (dddd, $J_{CF} = 254.1, 18.0, 13.4, 5.4$ Hz), 142.4 (dtt, $J_{CF} = 257.9, 13.2, 5.0$ Hz), 143.9 (dddd, $J_{CF} = 252.9, 16.0, 8.0, 4.0$ Hz), 148.2, 183.7. MS (70 eV) 298 (M^+, 75), 297 (100), 250 (8), 131 (20), 103 (25), 77 (16). EI HRMS m/z calcd for $[M]^+$ $C_{15}H_7F_5O$ 298.0417, found 298.0410.

Acknowledgements

Financial support from the National Institutes of Health (R01GM067169) is gratefully acknowledged. Computations were supported by the Center for Computational Molecular Science and Technology at the Georgia Institute of Technology and under a National Science Foundation CRIF Award CHE-0443564.

Notes and references

1 G. J. Kavarnos, (1993) *Fundamentals of Photoinduced Electron Transfer* (VCH Publishers, New York).
2 J. F. Callan, A. P. de Silva and D. C. Magri, *Tetrahedron*, 2005, **61**, 8551.
3 A. P. de Silva, H. Q. N. Gunaratne, T. Gunnlaugsson, A. J. M. Huxley, C. P. McCoy, J. T. Rademacher and T. E. Rice, *Chem. Rev.*, 1997, **97**, 1515.
4 G. L. Closs and J. R. Miller, *Science*, 1988, **240**, 440.
5 R. A. Marcus and N. Sutin, *Biochim. Biophys. Acta*, 1985, **811**, 265.
6 D. Rehm and A. Weller, *Israel J. Chem.*, 1970, **8**, 259.
7 M. Kollmannsberger, K. Rurack, U. Resch-Genger, W. Rettig and J. Daub, *Chem. Phys. Lett.*, 2000, **329**, 363.
8 T. Hirano, K. Kikuchi, Y. Urano and T. Nagano, *J. Am. Chem. Soc.*, 2002, **124**, 6555.
9 L. Yang, R. McRae, M. M. Henary, R. Patel, B. Lai, S. Vogt and C. J. Fahrni, *Proc. Natl. Acad. Sci. U. S. A.*, 2005, **102**, 11179.
10 J. Cody, S. Mandal, L. Yang and C. J. Fahrni, *J. Am. Chem. Soc.*, 2008, **130**, 13023.
11 C. J. Fahrni, L. C. Yang and D. G. VanDerveer, *J. Am. Chem. Soc.*, 2003, **125**, 3799.
12 K. Rurack, J. L. Bricks, B. Schulz, M. Maus, G. Reck and U. Resch-Genger, *J. Phys. Chem. A*, 2000, **104**, 6171.
13 C. Hansch, A. Leo and R. W. Taft, *Chem. Rev.*, 1991, **91**, 165.
14 A. R. Katritzky and R. D. Topsom, *Chem. Rev.*, 1977, **77**, 639.
15 D. J. Craik and R. T. C. Brownlee, *Prog. Phys. Org. Chem.*, 1983, **14**, 1.
16 I. Morao and I. H. Hillier, *Tetrahedron Lett.*, 2001, **42**, 4429.
17 K. C. Gross and P. G. Seybold, *Int. J. Quantum Chem.*, 2001, **85**, 569.
18 K. C. Gross, P. G. Seybold, Z. Peralta-Inga, J. S. Murray and P. Politzer, *J. Org. Chem.*, 2001, **66**, 6919.
19 H. H. Büker, N. M. M. Nibbering, D. Espinosa, F. Mongin and M. Schlosser, *Tetrahedron Lett.*, 1997, **38**, 8519.
20 I. Hyla-Kryspin, S. Grimme, H. H. Bueker, N. M. M. Nibbering, F. Cottet and M. Schlosser, *Chem.–Eur. J.*, 2005, **11**, 1251.
21 M. Charton, *Prog. Phys. Org. Chem.*, 1971, **8**, 235–317.
22 S. Bohm, P. Fiedler and O. Exner, *New J. Chem.*, 2004, **28**, 67.
23 O. Exner and S. Böhm, *Coll. Czech. Chem. Commun.*, 2006, **71**, 1239.
24 J. J. Sullivan, A. D. Jones and K. K. Tanji, *J. Chem. Inf. Comput. Sci.*, 2000, **40**, 1113.
25 C. H. Suresh and S. R. Gadre, *J. Phys. Chem. A*, 2007, **111**, 710.
26 P. J. Smith and P. L. Popelier, *Org. Biomol. Chem.*, 2005, **3**, 3399.
27 Y. Simón-Manso, *J. Phys. Chem. A*, 2005, **109**, 2006.
28 X. Gironés and R. Ponec, *J. Chem. Inf. Model*, 2006, **46**, 1388.
29 I. Fernández and G. Frenking, *J. Org. Chem.*, 2006, **71**, 2251.
30 B. Galabov, S. Ilieva and H. F. Schaefer, *J. Org. Chem.*, 2006, **71**, 6382.
31 P. Politzer and J. S. Murray, *Theor. Chem. Acc.*, 2002, **108**, 134.
32 E. P. Serjeant, and B. Dempsey, (1979) *Ionization Constants of Organic Acids in Aqueous Solution* (Pergamon, Oxford).
33 J. Jover, R. Bosque and J. Sales, *QSAR Comb. Sci.*, 2007, **26**, 385.
34 D. A. Kraut, P. A. Sigala, B. Pybus, C. W. Liu, D. Ringe, G. A. Petsko and D. Herschlag, *PLoS Biol.*, 2006, **4**, e99.
35 J. T. Blair, M. R. V. Sahyun and D. K. Sharma, *J. Photochem. Photobiol. A*, 1994, **77**, 133.
36 B. Valeur, (2006) *Molecular Fluorescence* (Wiley-VCH, Weinheim).
37 Y. Shao, L. F. Molnar, Y. Jung, J. Kussmann, C. Ochsenfeld, S. T. Brown, A. T. B. Gilbert, L. V. Slipchenko, S. V. Levchenko, D. P. O'Neil, R. A. DiStasio, R. C. Lochan, T. Wang, G. J. O. Beran, N. A. Besley, J. M. Herbert, C. Y. Lin, T. Van Voorhis, S. H. Chien, A. Sodt, R. P. Steele, V. A. Rassolov, P. E. Maslen, P. P. Korambath, R. D. Adamson, B. Austin, J. Baker, E. F. C. Byrd, H. Dachsel, R. J. Doerksen, A. Dreuw, B. D. Dunietz, A. D. Dutoi, T. R. Furlani, S. R. Gwaltney, A. Heyden, S. Hirata, C. P. Hsu, G. Kedziora, R. Z. Khalliulin, P. Klunzinger, A. M. Lee, M. S. Lee, W. Liang, I. Lotan, N. Nair, B. Peters, E. I. Proynov, P. A. Pieniazek, Y. M. Rhee, J. Ritchie, E. Rosta, C. D. Sherrill, A. C. Simmonett, J. E. Subotnik, H. L. Woodcock, W. Zhang, A. T. Bell, A. K. Chakraborty, D. M. Chipman, F. J. Keil, A. Warshel, W. J. Hehre, H. F. Schaefer, J. Kong, A. I. Krylov, P. M. W. Gill and M. Head-Gordon, *Phys. Chem. Chem. Phys.*, 2006, **8**, 3172.
38 A. D. Becke, *J. Chem. Phys.*, 1993, **98**, 5648.
39 C. T. Lee, W. T. Yang and R. G. Parr, *Phys. Rev. B*, 1988, **37**, 785.
40 J. N. Demas and G. A. Crosby, *J. Phys. Chem.*, 1971, **75**, 991.

